Refining Control, Charging, and Battery Chemistry for CO_2e Savings in Heavy-Duty Off-Road Plug-In Series Hybrid

Bryant Goodenough[1], Alexander Czarnecki[1], Darrell Robinette[1], Jeremy Worm[2], David Subert[2], Dylan Kiefer[2], Matthew Heath[2], Bob Brunet[2], Robert Kisul[2], Phil Latendresse[3], John Westman[3], and Andrew Black[4]

[1]Michigan Technological University, USA
[2]Michigan Technological University, APS LABS, USA
[3]Pettibone/Traverse Lift LLC, USA
[4]Soli Consulting LLC, USA

Abstract

With current and future regulations continuing to drive reductions in carbon dioxide equivalent (CO_2e) emissions in the on-road industry, the off-road industry is also likely to be regulated for fuel and CO_2e savings. This work focuses on converting a heavy-duty off-road material handler from a conventional diesel powertrain to a plug-in series hybrid, achieving a 49% fuel reduction and 29% CO_2e reduction via simulation. Control strategies were refined for energy savings, including a regenerative braking strategy to increase regenerative braking and a load-following hydraulic strategy to decrease electrical energy consumption. The load-following hydraulic control shuts off the hydraulic electric machine when it is not needed – an approach not previously seen in a load-sensing, pressure-compensated system. These strategies achieved a 24.1% fuel savings, resulting in total savings of 61% in fuel and 41% in CO_2e in the plug-in series compared to the conventional machine. Beyond control strategies, this study evaluated battery chemistry and charging strategy refinements for total cost of ownership (TCO) and lifetime CO_2e. LFP batteries emerged as the most cost-effective and least emitting due to their longer lifespan, which reduced replacement frequency. Charging comparisons showed that Level 2 charging (L2C) typically resulted in lower TCO but higher lifetime CO_2e than DC fast-charging (DCFC). DCFC costs were heavily influenced by local demand charges, and DCFC emissions were heavily influenced by local grid emissions.

Introduction

While significant investments have been made in on-road electrification, the off-road industry has not received the same level of investment [1]. The off-road sector represents a significant portion of emissions, accounting for 9% of total transportation emissions [2]. Hybrid electric powertrains are becoming more common in off-road equipment as energy savings from electrification technologies are realized [3]. Increasing emissions regulations are responsible for the investment in electrification technologies [1], and these regulations are expected to continue driving significant investment in electrification and other CO_2-reducing technologies. The California Air Resources Board is currently working on Tier 5 standards for off-road diesel engines [4], which are expected to include nitrogen oxide standards 90% more stringent than Tier 4 standards, particulate matter standards 75% more stringent than Tier 4, and, for the first time, CO_2 reduction requirements for off-road diesel engines [4]. While these regulations are specific to the engine manufacturer, original equipment manufacturers (OEMs) in the off-road sector may need to demonstrate reductions in overall emissions in the future. Electrification is a main avenue explored to achieve fuel savings [5]. This article will explore a plug-in series hybrid application for a heavy-duty off-road material handler, the Pettibone Cary-Lift 204i. Figure 1 shows the schematics and photos of the plug-in series hybrid and the base conventional machine, highlighting their distinct configurations while showcasing their similar external appearances. The control strategies will be explored to determine areas to reduce fuel and energy consumption through rule-based control modifications. Also, battery chemistry options and charging strategies will be explored to determine the lowest total cost of ownership (TCO) and lifetime carbon dioxide equivalent (CO_2e) values.

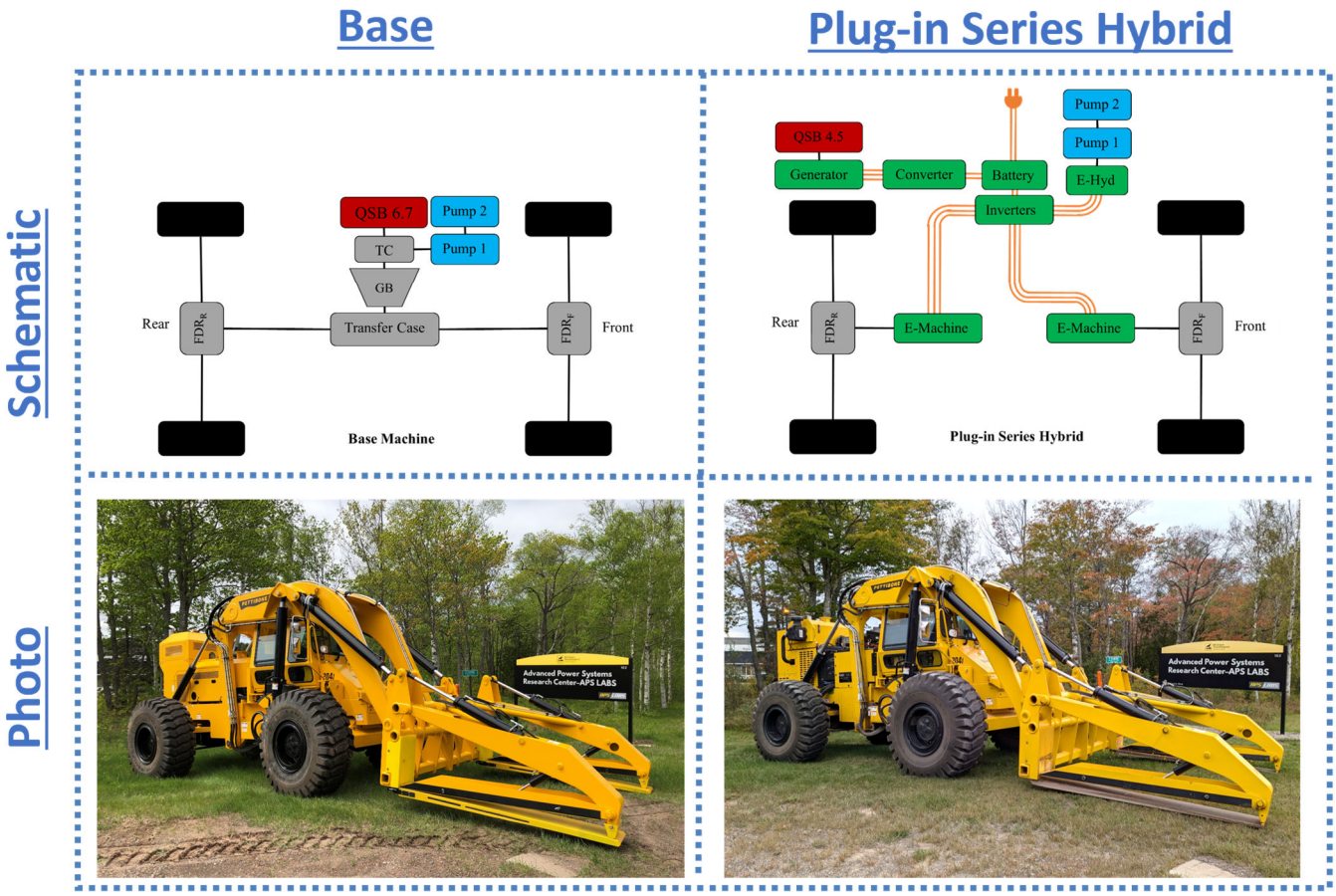

Figure 1. Schematics and photos of base conventional machine and plug-in series hybrid machine. Plug-in series hybrid with base control achieves 49% fuel and 29% CO_2e savings compared to base conventional machine. Adapted with permission from Ref. [6]; copyright SAE International.

Research articles focusing on heavy-duty off-road series hybrids are numerous, with some examples in references [3, 5, 7-13]. However, when further narrowing the search for articles focusing on heavy-duty off-road plug-in series hybrids, the authors have not found any references, as the plug-in capability further distinguishes this machine. This paper adds a unique plug-in series hybrid electrification architecture to the heavy-duty off-road space while exploring methodologies to reduce fuel and energy consumption through control modifications. Control modifications are often pursued for energy savings in off-road hybrids, as in [7-10], but this article adds new material to the control space by introducing a novel load-following hydraulic control that achieves 17.8% fuel savings compared to a continuously spinning system. While plenty of papers have been published on electrified hydraulic systems [14-26], none have been found to use a load-following system that allows for the pumps to be speed-controlled based on demand, and stopped when they are not needed. This unique system is explored in the section Control Refinement for Hydraulics: Load-Following.

This paper begins with a literature review exploring off-road electrification control and strategies before moving into a description of the modeling and analysis of the machine. Then, basic rule-based controls are discussed for the engine control, regenerative braking, and hydraulic control before moving into refined rule-based control of the regenerative braking and the hydraulic system for significant energy savings. Then, the paper zooms out to an architecture level, looking at options to reduce fuel and CO_2e by selecting different battery chemistries and charging strategies to compare the best options on a lifetime carbon dioxide equivalent (CO_2e) and total cost of ownership (TCO) basis.

Literature Review

Control strategies can be broken down broadly into rule-based and optimization-based control [5]. Rule-based control methodologies are often used in the development of a machine and can later be compared to more advanced control methodologies, as seen in [3, 9]. Rule-based control methodologies can also be modified for a reduction of fuel consumption, as in [27], where a plug-in hybrid tractor used a multi-mode fuzzy logic controller for fuel savings of up to 18%. Rule-based strategies can be modified based on knowledge of the system, and they can also be modified based on external optimization analyses [5]. Besides rule-based control strategies, optimization-based control strategies are used to determine the optimal results by minimizing fuel consumption, for example, using cost functions and constraints [5]. Global optimization strategies, like dynamic programming, achieve the global optimum result in a system but are not implementable in real-time because of the need for knowledge of the exact future driving cycle [9]. While many optimization-based control strategies are not real-time implementable, equivalent consumption minimization strategy (ECMS), pontryagin minimum principle (PMP), and model predictive control (MPC) have all been applied for real-time optimization applications [28]. This work will focus on refining rule-based control strategies based on knowledge of the system and identifying areas for improvement.

Hydraulic systems can represent significant portions of the overall fuel consumption of a heavy-duty off-road machine, with up to 26% of the overall fuel consumption going to the hydraulic system in the Cary-Lift specifically [29]. Different methods have been pursued to achieve fuel savings in hydraulic systems, with some of those

methods including changes in system design, reducing losses, and improving components and functions [17]. In hydraulic applications where electrification is added, energy regeneration can be used through potential energy recovery [17]. This has been seen in the heavy-duty off-road space on excavators [18, 19]. Other hydraulic systems look at the use of electro-hydraulic actuators for significant energy savings with up to 84.7% efficiency [21], but these can be limited due to the lack of adequate load-holding capability and power limitations [22]. The system of interest in this study requires counterbalance valves for safety considerations (load-holding). These counterbalance valves require hydraulic pressure to push the lifting cylinders down, eliminating the possibility of pursuing potential energy recovery. However, with an electric machine powering the hydraulic pumps, energy savings can come from following the required load rather than constantly spinning the hydraulic pumps, as is performed in many hydraulic systems.

The machine studied in this paper uses variable displacement pumps with pressure compensation, and the hydraulic pumps are powered by an electric machine that is kept constantly spinning so the hydraulic system can respond to changes in demand due to hydraulic activity. This constantly spinning system is analogous to the baseline system where the pumps are mechanically coupled to the engine and thus constantly spinning, however, this leads to excessive energy consumption when hydraulic movement is not required. A load-following system was desired so the electric machine powering the pumps was only turned on when there was a required hydraulic load to be met, and the speed of the electric machine was varied to best accommodate that hydraulic load. In [23], a load-following system was presented where an electric machine's speed was paired to a fixed displacement pump, and the speed was adjusted based on the system pressure to maintain constant pressure in a hydraulic press-brake. Another source analyzed electro-hydraulic actuators for variable speed and variable displacement hydraulic systems [24]. The system maintains a desired load pressure by adjusting pump speed and swashplate position [24]. In [25], a load-following system is explored with a variable displacement, pressure-compensated pump driven by an electric motor. The idle power consumption is reduced by lowering pump speed, but the pump is not turned off [25]. Also, [26] explores reducing pump speed at idle conditions. The work in this paper is distinguished from others due to the ability to turn off the pumps when in an idling condition.

Regenerative braking strategies are numerous in the field of electrified vehicles as a means of increasing efficiency and range [30]. Various methods are pursued to perform regenerative braking most efficiently, with strategies including fuzzy logic control, neural networks, model predictive control, sliding mode control, and adaptive control [30]. While many of these strategies work to optimize the regeneration for maximizing the amount of energy regenerated, more simple strategies using rules were pursued in this work and are explored in the sections Rule-Based Control for Regenerative Braking and Control Refinement for Regenerative Braking sections.

Charging strategies for electrified vehicles and machines include multiple options like Level 1 charging, Level 2 charging, and DC fast charging [31]. One study examined different charging strategies and their effect on cost and greenhouse gas emissions (CO_2e), where it found that different charging price strategies, like those that influence the timing of charging, can significantly impact greenhouse gas emissions [31]. The total cost of charging activities has been explored in the U.S. for light-duty vehicles, looking at a 15-year lifetime in [32], where it was found that the cost to charge an electric vehicle varies widely based on location, use, charging behavior, and equipment cost. An analysis of electric vehicle charging costs has also been performed in Europe, where similar conclusions were made that the cost varies widely [33]. These articles are concerned with light-duty electric vehicles, where the work in this paper will focus on a heavy-duty off-road machine and analyze the total cost of ownership (TCO) and CO_2e emissions over a 15-year lifetime, including Level 2 charging (L2C) and DC fast charging (DCFC). This work builds off of work performed in [6], where lifetime analyses were performed for total cost and CO_2e emissions for a heavy-duty off-road machine.

Different battery chemistries can yield vastly different performance and lifetimes for lithium-ion batteries [34]. A low battery lifetime can lead to much higher cost and CO_2e values for electrified vehicles compared to their non-electrified counterparts, as explored in [6], where a battery electric machine was found to have a much higher cost than a base conventional machine. The work in this paper considers different battery chemistries in a TCO and CO_2e perspective, introducing NCA and LFP battery options to the NMC battery used in [6].

Modeling of Plug-in Series Hybrid

Description

A high-fidelity plug-in series hybrid model was built in Simcenter Amesim to accurately represent the fuel and energy consumption of the series hybrid version of the heavy-duty off-road machine. The focus is on control and strategy modifications for energy savings using this high-fidelity model.

Refer to Figure 1 for the schematic representation of the plug-in series hybrid architecture and the schematic representation of the base machine. The base machine represents the conventional stock configuration, and the plug-in series hybrid represents the prototype that was built to demonstrate fuel savings. This paper explores the plug-in series hybrid.

Operating Cycles

Description

The model of the machine needed to be simulated on a representative operating cycle to understand possible fuel and energy savings. The energy savings depend on the machine's expected operation. To quantify the potential savings, custom operating cycles were developed to represent the typical operation of the base machine [29]. The three primary operations in a typical application include examples like loading large items onto a truck, unloading items from a railcar, or transporting from one location to another at a worksite [29]. These operating cycles are shown in Figure 2, with the speed values on the left y-axis and the hydraulic pump power values on the right y-axis.

These three operating cycles were combined and weighted along with idle time to create an overall time-weighted operating cycle, as seen in Figure 2. The percentage of time contributions for each of these events was determined by operational data from and conversations with Pettibone. This time-weighted operating cycle forms the basis for the fuel and CO_2e savings to be explored later in this paper. An 8-hour operation is assumed, with time percentages per operation based on this time-weighted operating cycle pie chart.

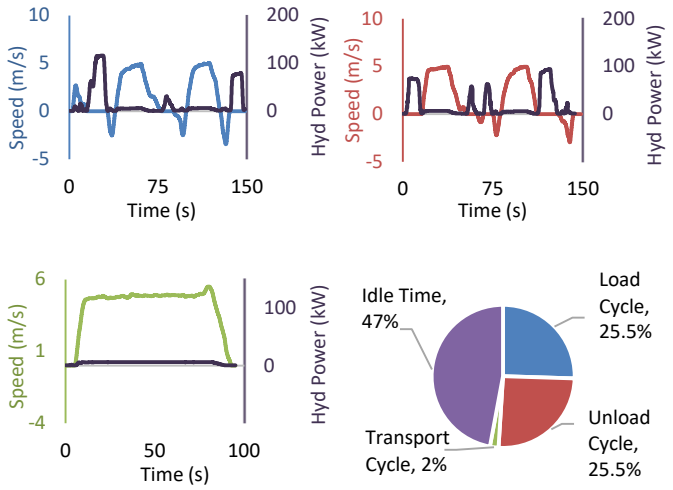

Figure 2. Load operating cycle (top left), unload operating cycle (top right), transport operating cycle (lower left), and time-weighted operating cycle (lower right). Reprinted with permission from Ref. [29]; copyright SAE International.

Rule-Based Control

Description

A rule-based control system was developed to represent the first level of control to be built into the physical machine. These rule-based controls were kept simple to retain a similar operability to the base machine. Also, the rule-based controls are simpler to implement onto the plug-in series hybrid, allowing for quicker implementation into the experimental machine. See Figure 1 for a picture of the completed plug-in series hybrid machine onto which the rule-based control was added.

The analysis to follow will provide details on the rule-based control implementation in the hybrid model of the machine in Amesim. The systems discussed include rule-based control methods for battery charging, hydraulic operation, and regenerative braking.

Analysis

Thermostatic Rule-Based Control of Battery SOC

The plug-in series hybrid architecture utilizes a 73.5 kWh-nominal lithium-ion Nickel Manganese Cobalt (NMC) battery. This battery was chosen to operate in the range of 20% to 90% state of charge (SOC), based on recommendations from the battery manufacturer and to reduce degradation. This battery is assumed to be recharged to 90% every night using level 2 charging from the grid after operating on an 8-hour shift during the day, following the time-weighted operating cycle per Figure 2.

During operation, the machine begins by running in charge-depleting (CD) mode, depleting the battery from 90% SOC down to 20%. After hitting the 20% minimum, the engine turns on and recharges to 25% before turning off and depleting to 20%. This is a thermostatic rule-based control, where the engine turns on to increase battery SOC for a period of time before turning off and allowing SOC to deplete. Thermostatic rule-based control was chosen because of the simplicity of implementation and because of the aftertreatment system, where frequent on/off cycling of the engine in a different control strategy could lead to higher emissions due to an inability of the aftertreatment system to reach and sustain adequate temperature.

Since this is a series hybrid machine both in the propulsion system and the hydraulic system, the engine is not mechanically linked to the vehicle movement or hydraulic movement (see Figure 1). This means the engine can operate at any point within its speed and torque limits. As such, the point of maximal system efficiency was targeted, so the engine consumed the least amount of fuel while recharging the battery. This point of maximal system efficiency considered the efficiencies of the engine, generator, inverter, and battery charging. A torque coupler was used to connect the engine to the generator, so the limitations of this coupler were used to bound the region of operation. See Figure 3 for this overall efficiency plot, including the torque coupler's no-fly zones.

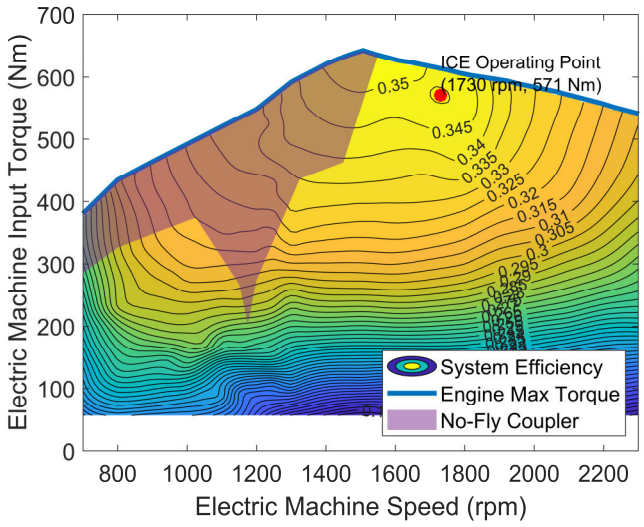

Figure 3. Overall system efficiency, including the efficiencies of the engine, generator, inverter, and battery. Assuming 25°C battery temperature at 20% SOC.

The engine operating point, as seen in Figure 3, was chosen in the middle of a high-efficiency island with around 35.0% overall efficiency[1], occurring at the engine operating point of 1730 rpm and 571 Nm for 103 kW of engine power. This operating point was chosen due to its high-efficiency value and relative isolation from the no-fly region of the coupler. Other points of slightly higher efficiency are possible up to about 35.3% at 1550 rpm and 625 Nm of torque, but these points were close to the no-fly regions of the coupler and hence were avoided.

Rule-Based Control for Hydraulic System: Continuously Spinning

The next system for which rule-based control was used is the hydraulic system, which is responsible for lifting up to 9,100 kg (20,000 lb.) of material to a maximum height of 4.0 m (13 ft) [29]. This high lifting capacity requires a powerful hydraulic system, where pump power values reach as high as 120 kW during portions of the load operating cycle, as in Figure 2.

[1] Recall, Figure 3 is ***overall efficiency*** which includes the engine, generator, inverter, and battery, not just engine efficiency.

The base hydraulic system of the machine was mostly unchanged in the plug-in series hybrid, with the largest change being the pumps were powered by an electric machine rather than the engine. The base system is a load-sensing, pressure-compensated system that powers the material handling, steering, and braking systems, and these functions were all retained for the electrified hydraulic architecture. See Table 1 for more hydraulic system parameters and Figure 4 for a simplified hydraulic system sketch.

Table 1. Hydraulic system parameters for base machine. These needed to be matched for the plug-in series hybrid.

Hydraulic System Parameter	Specification
System Type	Load-sensing, pressure-compensated
Maximum System Pressure	148 bar (2150 psi)
Maximum Lift Capacity	9,100 kg (20,000 lb.)
Maximum Lift Height (Fully Loaded)	4.0 m (13 ft)
Hydraulic Tank Volume	284 L (75 U.S. gal)
Hydraulic Fluid	ISO VG 32 Hydraulic Oil
Number of Pumps	2 (in series)
Hydraulic Pump Displacement (each)	100 cc/rev
Minimum Pump Speed	600 rpm
Maximum Pump Speed	2500 rpm
Maximum Pump Power Required	120 kW, in load cycle

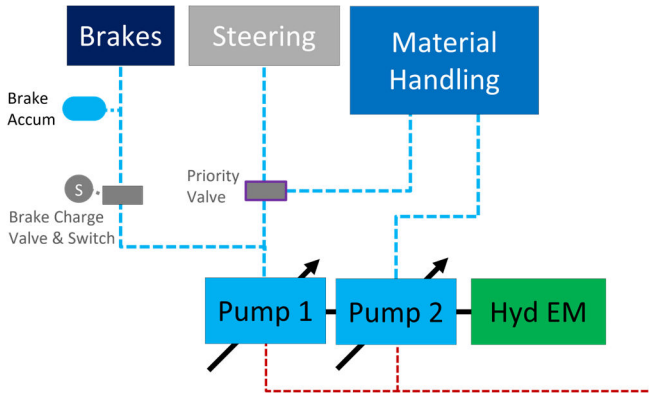

Figure 4. Simplified representation of continuously spinning rule-based plug-in series hydraulic system.

The plug-in series hybrid was aimed at replicating as much of the base machine as possible to match the performance of the base machine, so the operation was familiar to the operators. The continuously spinning hydraulic system followed this logic, pursuing a strategy mimicking the base machine, where the hydraulic pumps continuously spin. In the base machine, the pumps were powered by a power take-off (PTO) from the engine, which meant that if the engine was spinning, the pumps were spinning, and spinning at a rate directly related to engine speed. The base machine's hydraulic system was retained in its entirety, with the only change being that the pumps were powered by an electric machine rather than by the engine's PTO.

In the plug-in series hybrid model, the continuously spinning system followed the engine speed of the base machine to match this base operation, with a lower speed at idle conditions to save energy. See the comparison between these systems in Figure 5.

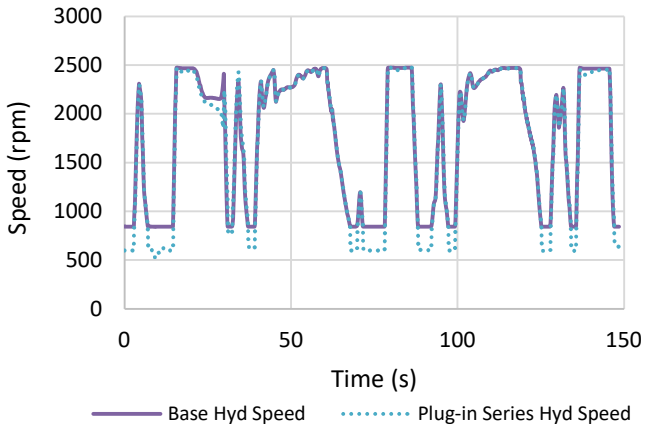

Figure 5. Pump speed comparison of base hydraulic system and plug-in series hybrid rule-based hydraulic system (continuously spinning) during load operating cycle.

The hydraulic performance of the base machine was calibrated and validated using experimental data, as elaborated in [29]. Given the close similarity between the base and continuously spinning systems (see Figure 5), there is confidence in the accuracy of the modeled hydraulic control of the continuously spinning system.

Rule-Based Control for Regenerative Braking: Baseline Regen

With a maximum ground speed of 8.9 m/s (20 mph) the machine does not achieve high speeds relative to a light-duty vehicle, however, the large machine mass of 23,000 kg (50,000 lb.) unloaded means that regenerative braking can be beneficial for recharging the battery. This led to the development of a rule-based regenerative braking strategy that once again focused on simplicity and similarity to the base machine.

The base machine does not have a brake pressure sensor, but the brake pedal position (BPP) is known as a binary 0 or 1 (off or on) based on the digital input to the brake lights. This information is used to see when the brakes are applied, but the extent to which those brakes are applied is unknown. Taking this into account, regenerative braking should not increase drastically when the brake position goes from off to on because drastic increases could lead to large decelerations for a light brake application.

The regenerative braking values in the rule-based control were chosen to match the deceleration of the base machine's engine braking when coasting down from the top speed of 8.9 m/s (20 mph) when the accelerator pedal position (APP) was zero in 4th (top) gear. The matching of the regenerative braking happens until about 3.5 m/s (7.8 mph), at which point the base machine achieves idle engine speed and begins to coast with less resistance due to a lack of engine braking at these lower speeds, as seen in Figure 6. The plug-in series hybrid continues regenerative braking until 1.6 m/s (3.6 mph), corresponding to an assumed minimum motor speed of 500 rpm for effective regeneration.

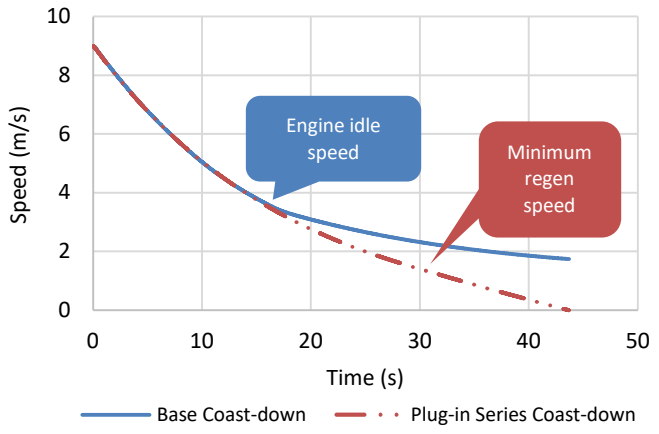

Figure 6. Coast-down comparison between base machine engine braking and plug-in series regenerative braking. The base machine nears idle engine speed at 3.5 m/s in 4th gear, and the plug-in series hybrid stops regeneration at 1.6 m/s (500 rpm motor speed).

This rule-based control of regenerative braking could be further tuned to match the base engine braking at all speeds, but this would mimic the lower deceleration seen as the engine reaches idle speed, which is not a desirable trait since the machine will continue indefinitely. As such, the regenerative braking strategy was chosen so that a zero APP nearly matched the zero APP of the base machine while coasting from the top speed of 8.9 m/s (20 mph) to 3.5 m/s (7.8 mph).

The braking signal was also used to increase regenerative braking, so that when the brakes were applied, the regenerative braking value was doubled. This value was chosen initially because it does not yield a drastic increase in deceleration that could create an unpredictable braking situation for the operator. See Figure 7 for the regenerative torque values.

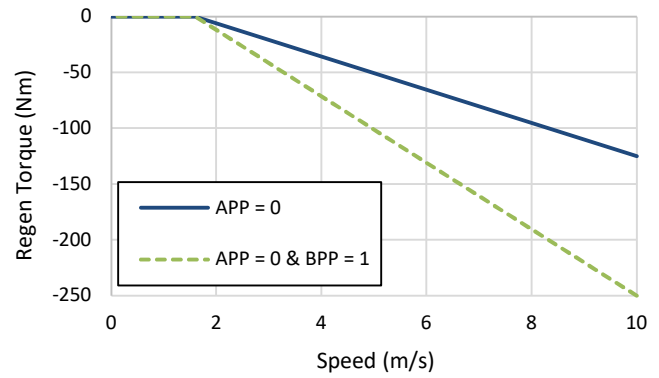

Figure 7. Regenerative braking torque at zero accelerator pedal position (APP) and at zero APP with zero brake pedal position (BPP). Torque values are per electric machine; multiply by 2 for total regen torque.

Incorporating the thermostatic rule-based control of battery SOC with rule-based control of the hydraulic system and the rule-based control of the regenerative braking yielded a daily fuel consumption of 40.0 L and emissions of 172 kg CO_2e over the time-weighted operating cycle from Figure 2. Further fuel and CO_2e savings can be achieved by looking at other control methodologies and charging strategies, as explored in the upcoming sections.

Refined Rule-Based Control for Fuel Savings

Description

The previous sections introduced the concepts of thermostatic rule-based control of battery SOC, rule-based control of the hydraulic system, and rule-based control of the regenerative braking strategy. This section explores the potential for fuel and energy savings by refining the control of the hydraulic system and the regenerative braking strategies. The thermostatic rule-based control of the battery SOC remains the same.

These refined rule-based methodologies are aimed at being simple modifications for significant additional fuel savings. With minimal changes in the plug-in series hybrid, these strategies can achieve significant fuel and energy savings, as explored in the upcoming analysis.

Analysis

Control Refinement for Hydraulics: Load-Following

The initial hydraulic control was implemented such that the pumps were continuously spinning with a minimum idle speed of 600 rpm, as noted in Figure 5. As seen in Figure 2, the idle time comprises almost half of all of the operation of the machine, meaning turning off the electric machine during these periods of inactivity could yield substantial fuel and energy savings. This led to the development of a hydraulic system that could turn off the hydraulic electric machine when it was not needed, and would turn back on when a hydraulic event was requested. The system layout is presented in Figure 8.

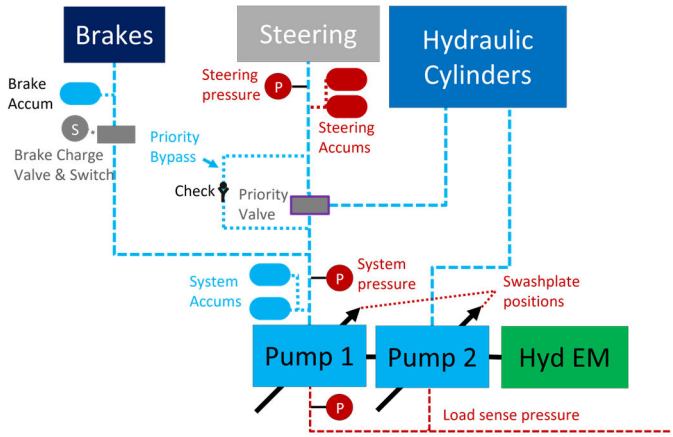

Figure 8. Simplified representation of the load-following plug-in series hydraulic system. Compare to the continuously spinning system in Figure 4.

Achieving a load-following hydraulic system required adding multiple 3.79 L (1 U.S. gallon) accumulators, two for the main system and two for the steering system. These are added as pressure reservoirs to perform smaller hydraulic actions and to begin moving cylinders when the hydraulic electric machine is accelerating up to desired speed. For example, the steering accumulators could power the machine's steering without requiring the pumps to be turned on. A priority valve bypass was also added, which allows pump flow to go around the priority valve and charge the steering system's accumulators rather than being diverted to the hydraulic cylinders.

The load-sense (LS) pressure comes from the directional control valves for each of the hydraulic components, like the material handling cylinders' valves, the steering valve, or the brake charge valve. For example, when an operator moves the joystick to lift

material, hydraulic fluid goes to the valve to move the cylinder. This fluid also has a pressure that goes to the load-sense gallery, where all load-sense pressures are compared, and the highest pressure reaches each of the pumps. This load-sense pressure tells when a hydraulic component requires flow and indicates if the hydraulic electric machine needs to be turned on and when it can be turned off.

This load-following system was designed to maintain performance and similarity to the base machine while reducing the energy consumption of the hydraulic system. The hydraulic performance was compared in each operating cycle to ensure the load-following and continuously spinning control strategies adequately matched the base machine's hydraulic performance. Once this was confirmed for each of the operating cycles for each hydraulic cylinder, the energy consumption values were compared for each cycle, as seen in Figure 9. This looks at the electrical energy going into the hydraulic electric machine.

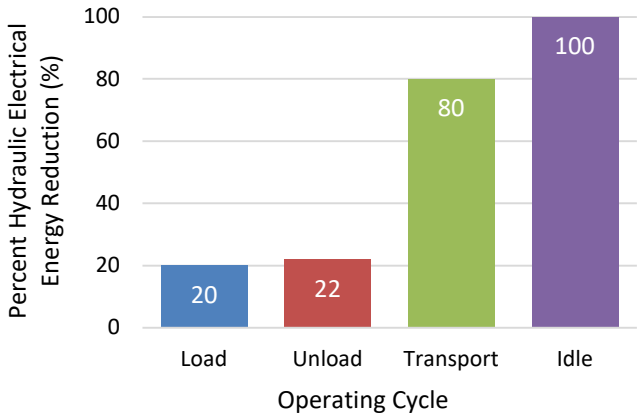

Figure 9. Hydraulic electric machine electrical energy consumption reduction for each operating cycle, comparing load-following control to continuously spinning control.

Once each operating cycle was confirmed, the next step was evaluating the overall energy consumption from the 8-hour time-weighted operating cycle (Figure 2). The results show a notable decrease in overall electrical energy consumption from the load-following system with a 24.8% reduction. These significant savings are possible due to the ability to turn off the electric machine when it is not necessary. In the continuously spinning control scheme, the hydraulic electric machine is always powered on and spinning at 600 rpm or higher, while the load-following system has many periods where it turns off entirely, like in between hydraulic actions or during idle time. Also, the addition of accumulators to the hydraulic system has further enabled the electric machine to be switched off as the accumulators can provide a pressure reservoir to perform minor hydraulic activities.

The control logic for this load-following system considered the system pressure, steering pressure, swashplate position, and load-sense pressure, with these sensors labeled in Figure 8. These inputs were then used to determine when the hydraulic electric machine should be turned on, when it should be turned off, and how the speed should be determined. Figure 10 shows the stateflow logic used to control the hydraulic electric machine in the load-following system.

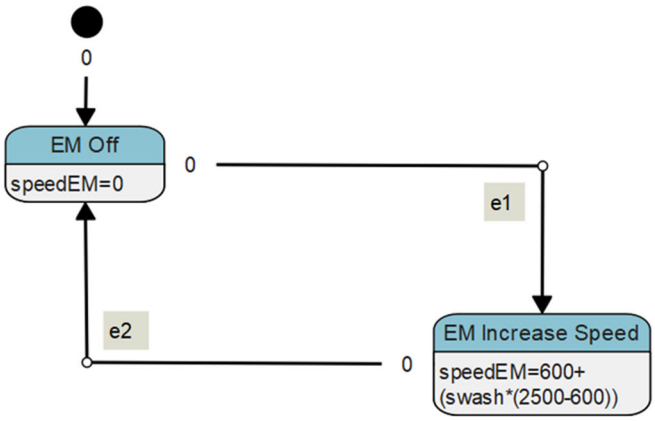

Figure 10. Stateflow logic used to control the load-following hydraulic system. e1 and e2 represent transitions to the on state and the off state, respectively. Pressures are in units of psi, speed is in units of rpm, and the swashplate position is the fractional displacement.

This load-following hydraulic control was performed with active closed-loop speed control of the hydraulic electric machine. A higher swashplate led to a higher hydraulic electric machine speed, meaning the speed was adjusted according to the instantaneous demand.

The values for the limits to turn on or off the electric machine were chosen iteratively based on hydraulic system performance. The system pressure, for example, should maintain at least 1000 psi (68.9 bar) if there is a load-sense (LS) pressure over 100 psi (6.89 bar), indicating a hydraulic event is occurring. These values could be further tuned for better controllability of the hydraulic functions or for lower energy consumption.

The load-following system was designed to integrate into the plug-in series hybrid machine. As such, it is expected that the values chosen for the control would be modified on the experimental machine based on what achieves the best performance in experimentation.

Control Refinement for Regenerative Braking: Threshold-Based Brake Management (TBBM)

The original rule-based control of the regenerative braking strategy looked at a linear regenerative torque that decreased with speed and was multiplied by two when the brakes were applied. For this section, the regenerative braking control was refined by introducing a threshold-based brake management (TBBM) control logic where regenerative braking was used for all braking events equal to or above 500 rpm motor speed, and friction brakes were used for all braking events below 500 rpm motor speed, as explained in Table 2.

Table 2. Control description of base and TBBM regenerative braking systems.

	Motor Speed < 500 rpm	Motor Speed > 500 rpm
Base Regen with Brakes Applied	All friction braking	Regen max. of 250 Nm per motor; rest by friction brakes
TBBM Regen	All friction braking	All regen braking

Figure 11 demonstrates the threshold-based brake management (TBBM) functionality compared to the baseline regenerative braking strategy. The TBBM braking strategy utilizes regenerative braking at

much higher power values, enabling more energy to recharge the battery pack, saving energy and fuel.

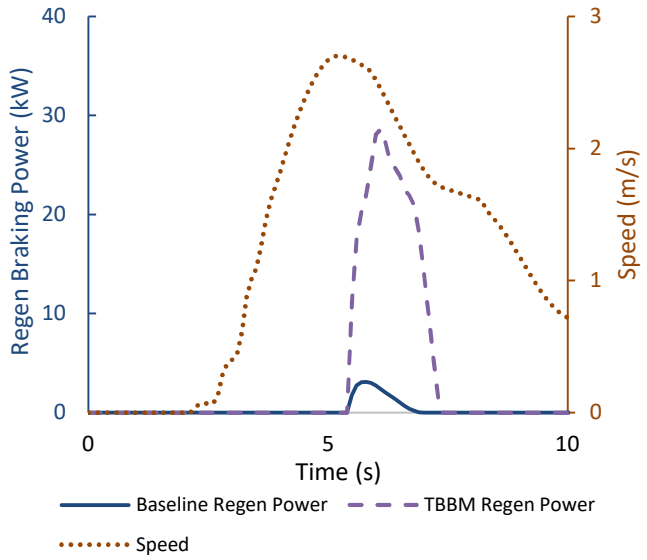

Figure 11. Regenerative braking power comparison between baseline regen and threshold-based brake management (TBBM) regen for first 10 seconds of load operating cycle.

Based on the braking event from Figure 11, the maximum possible energy recovery can be compared to the actual regenerated energy. The maximum energy recovery corresponds to the machine's kinetic energy (KE) at its peak velocity of 2.7 m/s during this period, slowing to 0 m/s, with a total mass of 23,212 kg.

$$KE = 0.5 \cdot m \cdot v^2 \tag{1}$$

Where,
m is the machine's total mass
v is the machine's maximum velocity

Substituting the values, the calculated KE is 84.6 kJ, representing the upper limit for regenerative braking energy recovery. In the simulation implementation, however, the braking energy recovery will be based on the time-based accumulation of motor braking torque, as seen in (2):

$$E_{Recovered} = \int_{t_0}^{t_f} (T_{em} \cdot \omega \cdot \eta)\, dt \tag{2}$$

Where,
T_{em} is the total electric motor torque
ω is the electric motor speed
η is the combined system efficiency

Simulation results indicate an actual energy recovery of 2.62 kJ for the baseline strategy and 36.8 kJ for the TBBM strategy at the tractive electric machines. When accounting for an assumed 87% combined efficiency for the electric machines and inverters along with a 97% battery charging efficiency[2], the regenerated braking energy into the battery becomes 2.21 kJ and 31.1 kJ for the baseline and TBBM strategies, respectively.

Through the entire 8-hour time-weighted operating cycle, the regenerated energy can be compared between the baseline and TBBM strategies, where higher values mean more energy going into the battery pack and lower energy and fuel consumption. Figure 12 illustrates these differences, where the TBBM braking strategy yields over three times the amount of energy as the baseline regenerative braking strategy. In the Applications section to follow, this regenerated energy is translated into fuel consumption values.

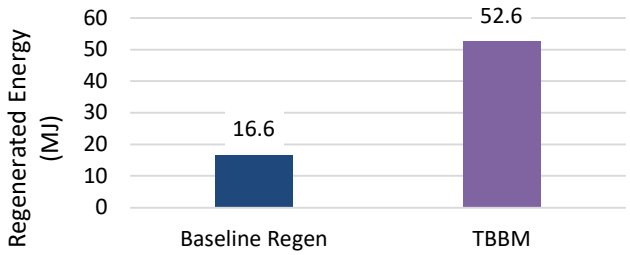

Figure 12. Regenerated energy comparison between baseline regen and TBBM, for the 8-hour time-weighted operating cycle. More regenerated energy means more energy going back into the battery.

Applications

The load-following hydraulics and TBBM regenerative braking strategies do not require large investments in new parts as they leverage the already present systems on the electrified machine. As manufacturers in the heavy-duty off-road space continue to pursue electrified options for their equipment, these low-cost control options that achieve large savings should be pursued to lower operating costs and carbon dioxide equivalent (CO_2e) emissions. Figure 13 shows the comparison of fuel consumption between the control methods mentioned above.

[2] Battery efficiency is based on the modeled power losses, determined by current and resistance, where the resistance of the battery is based on the SOC and temperature from manufacturer data.

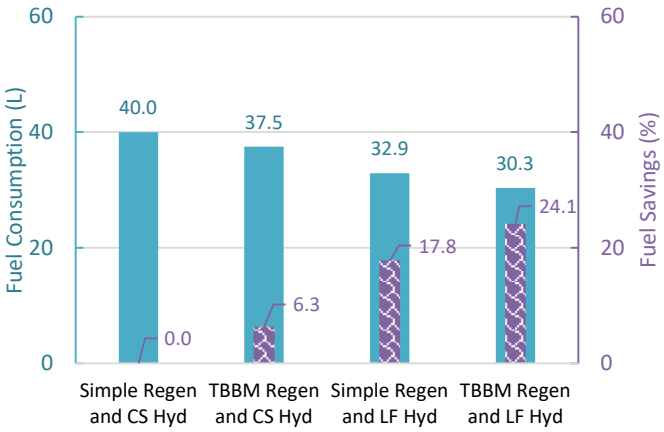

Figure 13. Fuel consumption and fuel savings for all control methods analyzed, on the 8-hour time-weighted operating cycle. Savings percentages are compared to base rule-based control with baseline regen and CS hydraulics. CS = Continuously Spinning, LF = Load-Following.

The fuel savings from integrating these different control methods are significant, with up to 24.1% additional fuel savings from including the TBBM with load-following hydraulics. The TBBM braking represents a 6.3% fuel savings compared to the baseline regen, and the load-following hydraulics represents a 17.8% fuel savings compared to the continuously spinning system. On a CO_2e basis, these control strategies combined lead to 142 kg CO_2e per day, down from 172 kg CO_2e per day in the base control (17.5% decrease). Compared to the base conventional machine, these savings amount to 61.0% fuel savings and 41.0% CO_2e savings.

Battery Chemistry and Charging Strategy Refinement

Description

Energy and emissions reductions could also be made on the machine architecture level, considering different battery chemistries or experimenting with different battery charging strategies. These considerations can change fuel consumption each day but become more important when looking at the machine's entire lifetime. This section aims to determine the battery chemistry and charging strategy that yields the lowest cost and lowest CO_2e emissions in the U.S. over the machine's 15-year lifetime.

The following analysis assumes the plug-in series hybrid uses the most basic control, with continuously spinning hydraulics and baseline regenerative braking, as discussed in previous sections. It also assumes that each battery chemistry can charge at a 2C charge rate for 30 minutes.

Different battery chemistries can vary widely in total lifecycles, yielding different costs and CO_2e over a lifetime when factoring in battery replacements. The battery chemistries to be explored in this section include Nickel Manganese Cobalt (NMC), Nickel Cobalt Aluminum (NCA), and Lithium Iron Phosphate (LFP). Battery charging strategies can also be leveraged to reduce fuel consumption and CO_2e production. For battery charging, Level 2 charging (L2C) will be compared to opportunity direct current fast charging (DCFC). L2C occurs overnight after the machine has operated for 8 hours during the day. Opportunity DCFC is at a 2C charge rate for each chemistry, coming near 150 kW of power into the battery. This DCFC occurs during breaks in the day, assuming two 10-minute breaks and one 30-minute lunch break, with charging also occurring overnight.

Each of these battery chemistries and charging strategies were compared to one another and to the base machine, which uses no form of electrification. Each option was also compared in different regions, looking at the baseload values for the U.S. average, Pennsylvania, Oregon, and Indiana. The U.S. average was chosen for a representative look at the entire U.S., and Pennsylvania was chosen due to the high volume of these machines in Pennsylvania. Oregon and Indiana represent the 15th and 85th percentile of electricity emissions in 2021 [35], which aids in the comparison of a cleaner grid to a dirtier grid. Table 3 displays the test matrix used in the following analysis.

Table 3. Test matrix for battery chemistry and charging strategy refinement study. Total of 28 options studied.

Machine Architecture	Battery Option	Charging Option	Region
Base	Not applicable	Not applicable	US PA OR IN
Plug-in Series	NMC NCA LFP	L2 Charge DC Fast Charge	US PA OR IN

Analysis

Battery lifetime depends on factors such as temperature, C-rate, chemistry, duty cycle, and more [34]. In this study, NMC, NCA, and LFP batteries are compared because these are chemistries commonly seen in vehicle applications. The battery performance and parameters were defined based on Amesim parameters for these chemistries along with manufacturer data from an NMC battery. Battery cost was assuming a 2021 cost of an NMC battery of $250/kWh [6], then adjusted for 2022 according to an International Energy Agency (IEA) report [36]. Battery lifetime assumptions are according to [34], which compared NMC, NCA, and LFP batteries based on C-rate and temperature. The battery lifetime comparison is seen in Figure 14. A comprehensive list of assumptions and parameters for the batteries is found in Appendix A.

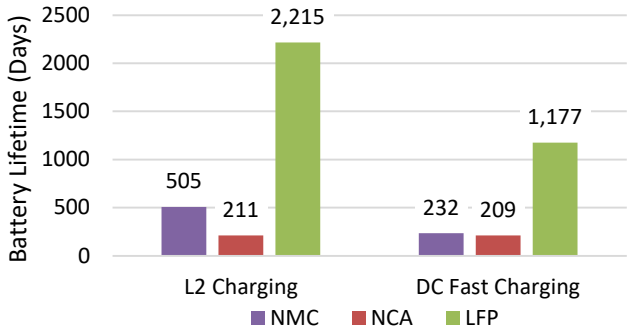

Figure 14. Battery lifetime comparison between different battery chemistries and charging strategies, on the 8-hour time-weighted operating cycle. Battery lifetime data from [34].

The battery lifetime affects the overall CO_2e emissions of these plug-in series hybrid architectures because of the necessity of battery replacements. These machines are expected to operate 8 hours a day for 260 days a year, which means operating time and hence charge and discharge cycles accumulate quickly, and battery replacements can occur regularly. From Figure 14, the NCA battery in the L2C

scenario will last less than 1 year, assuming 260 working days per year, whereas the LFP battery will last about 8.5 years.

The plug-in series hybrid was modeled in Amesim using the NMC, NCA, and LFP batteries, both with L2C and with opportunity DCFC. Figure 15 shows the fuel consumption comparison for each option on the 8-hour time-weighted operating cycle. Notice how the DCFC significantly reduces fuel consumption, with between 60 and 70 percent fuel savings depending on battery chemistry.

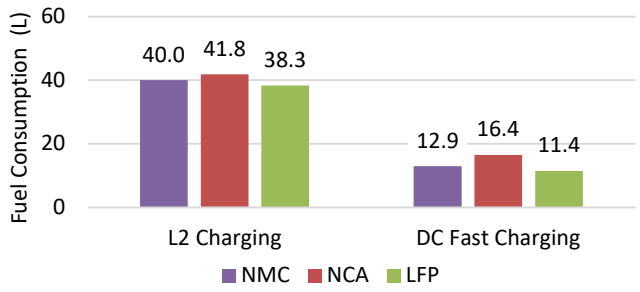

Figure 15. Fuel consumption comparison between different battery chemistries and charging strategies, on the 8-hour time-weighted operating cycle.

The DCFC achieved significant fuel savings due to the reduced reliance on the engine for recharging. Figure 16 shows the battery state of charge (SOC) traces for the different chemistries and charging strategies. The DCFC results in large SOC increases, with the lunch break enabling increases of SOC from around 20% to around 90%. L2C assumes charging only happens overnight, therefore no SOC increases are seen except for those required in charge sustaining mode.

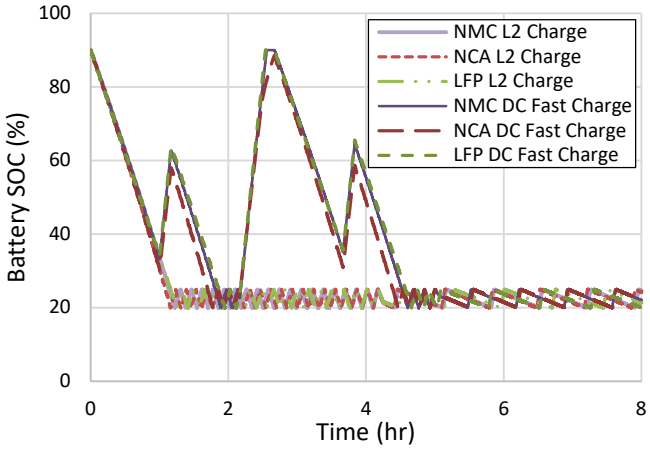

Figure 16. Battery SOC vs. time for different battery chemistries and charging strategies on the 8-hour time-weighted operating cycle. DCFC assumes two 10-minute breaks and one 30-minute lunch break.

Lifetime CO_2e Emissions

The carbon dioxide equivalent (CO_2e) emissions and cost were calculated for each of the chemistries and charging strategies to determine the chemistry and charging that would yield the lowest cost and the lowest CO_2e emissions. These are all compared to the base machine, and assume the base machine starts at zero emissions and zero cost. Purchasing parts like electric machines and batteries increases the initial cost and CO_2e of the plug-in series hybrid architectures. Maintenance events are also included for all chemistries and charging options. A full list of assumptions is found in Appendix B. A similar analysis was performed in [6], where lifetime CO_2e and cost were compared for several electrified architectures of the Cary-Lift. Figure 17 shows these lifetime CO_2e emissions.

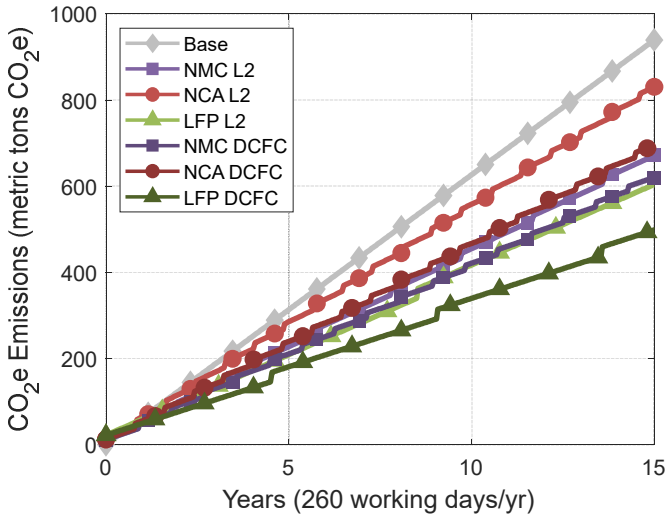

Figure 17. 15-year lifetime carbon dioxide equivalent (CO_2e) comparison between all battery chemistries and charging options, for U.S. average CO_2e. Base machine included for comparison purposes and represents an architecture without any electrification.

Figure 17 illustrates the differences in CO_2e emissions for the studied battery chemistries and charging strategies over the 15-year lifetime of the machine using U.S. average values. The highest CO_2e emissions come from the base machine due to its high fuel consumption. The lowest CO_2e emissions come from the LFP battery using DCFC. The LFP battery has the longest lifetime, requiring far fewer replacements than the other battery chemistries, and hence produces less CO_2e emissions for battery replacements. DCFC enables much lower fuel consumption, enabling more usage of the electricity grid and thus reducing overall CO_2e emissions.

Total Cost of Ownership

Cost was also analyzed to determine which chemistries and charging strategies were the most cost-effective. Maintenance events were also included in the cost, with the most notable costs associated with battery replacements. Engine and axle rebuilds are examples of maintenance events considered for all architectures. Charging infrastructure costs are not included in this analysis as it was outside of the scope of the work, but the costs of installing a DC fast charger are significant. Figure 18 shows the 15-year cost comparison for all chemistries and charging strategies for the U.S.

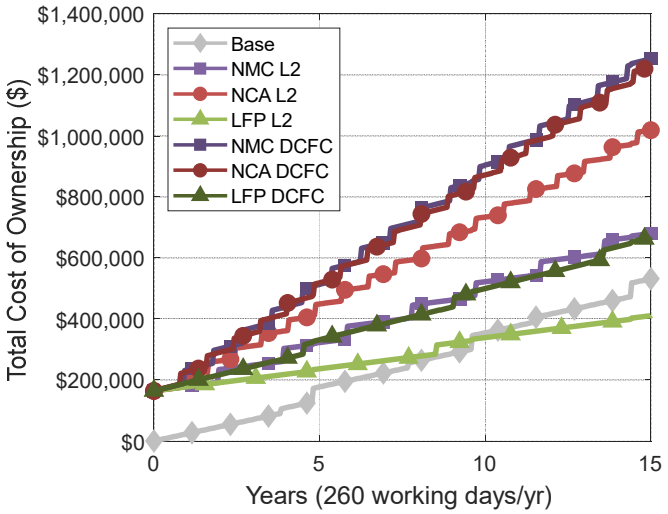

Figure 18. 15-year lifetime cost comparison between all battery chemistries and charging options, for U.S. average cost. Base machine included for comparison purposes and represents an architecture without any electrification.

The most expensive options are the NMC and the NCA batteries using DCFC. The NMC and NCA batteries have short lifetimes when using DCFC (see Figure 14), requiring frequent battery replacements. DCFC is expensive primarily due to demand charges, assumed at $15/kW per month based on an NREL report [37]. This demand charging cost increases electricity bills substantially, with a 150 kW charge at $15/kW yielding a $2250 demand charge per month, or $75 per day for only the demand charge. Adding electricity costs and diesel costs, the NCA battery with DCFC costs $103/day to operate, compared to the NCA battery with L2C which only costs $57/day to operate. This is highly dependent on demand charge rates, which vary substantially by region and by provider, ranging from $0/kW to over $30/kW per month [37]. The challenge of these demand charge rate discrepancies is addressed in the Total Cost of Ownership vs. Lifetime CO_2e section.

The LFP battery with L2C is the least expensive option, followed by the base architecture. The LFP battery is inexpensive due to infrequent battery replacements and large fuel savings.

Total Cost of Ownership vs. Lifetime CO_2e

After the results were determined for the lifetime CO_2e and total cost of ownership, the results were plotted together to determine the best options over a 15-year total lifetime. In Figure 19, the total cost of ownership is plotted against the lifetime CO_2e emissions, where the best options (lowest cost and lowest CO_2e) are to the lower left of the figure.

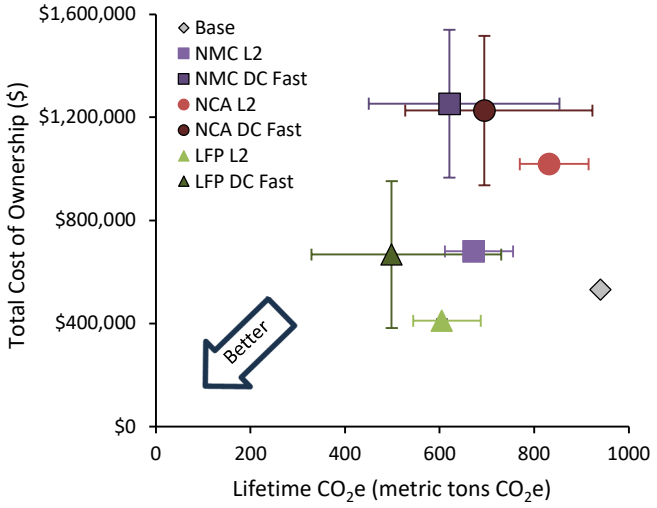

Figure 19. Total cost of ownership vs. lifetime CO_2e emissions over 15-year machine lifetime in the U.S., for all battery chemistries and charging options assuming $15/kW demand charge. Horizontal error bars represent CO_2e differences from charging in different regions, where high values (to right) are charging in Indiana, and low values (to left) are charging in Oregon. Vertical errors bars represent different demand charges, where upper error bars use a $30/kW demand charge, and lower error bars use a $0/kW demand charge.

From Figure 19, the best battery chemistry is the LFP battery, as it results in lower CO_2e emissions and lower total cost of ownership than the NMC and NCA batteries. This is driven mostly by its increased lifetime. An important caveat is that the LFP battery has a lower energy density, which requires a larger and heavier battery. In applications that are limited in packaging space and mass, an LFP battery may not work. See Appendix A for the volume and mass compared to the NMC and NCA batteries of similar voltages and capacities, where the LFP battery is over twice as voluminous and heavy. This paper assumed packaging space was not a constraint.

The best charging strategy (L2C or DCFC) is dependent on region, with horizontal error bars representing charging in Oregon (to left), and charging in Indiana (to right), with middle values being U.S. average values. Vertical error bars represent differences in cost from demand charges, with middle values using a $15/kW demand charge, upper values at $30/kW, and lower values at $0/kW. Demand charges are dependent on the region and the provider, and these can vary drastically from one region to another [37], hence the usage of lower and upper bounds. As evident from the large error bars in all DCFC scenarios in Figure 19, both CO_2e emissions and cost are dependent on the region of charging, as higher grid emissions and higher demand charges can drive up CO_2e and cost notably.

The best charging strategy needs to be analyzed for each application by looking at the demand charges for the location of charging and the expected grid emissions. Comparing the LFP L2C to the LFP DCFC in Figure 19, the DCFC scenario has the potential to produce less CO_2e while also being less expensive. It also has the potential to produce more CO_2e while being more expensive, depending on the region. The L2C strategy will likely be more effective for cost-sensitive applications. For CO_2e-sensitive applications, the DCFC scenario usually produces lower emissions, with the caveat that a dirtier grid has the potential to produce higher emissions than the L2C scenario.

Discussion

The results from this work are from simulations performed in Simcenter Amesim, using high-fidelity models of the machine in its plug-in series hybrid electrification architecture (Figure 1). The

results of this study indicate that significant savings are possible with control and architecture refinements. 17.8% fuel savings were observed by changing from continuously spinning hydraulics to load-following hydraulics, and 6.3% fuel savings were observed by changing from baseline regenerative braking to TBBM regenerative braking.

Looking at the battery chemistry and charging strategy refinement, the LFP battery was found to be the most promising due to its significantly improved lifespan. L2C was usually cheaper than DCFC when factoring in demand charges, but DCFC resulted in much lower emissions than L2C when using a cleaner electricity grid for charging. The superiority of DCFC versus L2C is highly dependent on the region in which the machine is being charged, as seen in Figure 19, so a thorough analysis of the electricity grid emissions and demand charges is required when selecting a charging strategy.

Conclusions

With future regulations likely to continue driving forward emissions reductions for off-road equipment, there is an increasing need for solutions to reduce carbon emissions [38]. This work analyzed a plug-in series hybrid version (Figure 1) of a heavy-duty off-road material handler. Further savings on the plug-in series hybrid were achieved by refining the basic rule-based control of the baseline regenerative braking system and the continuously spinning hydraulic system. Fuel savings of 6.3% and 17.8% were observed by introducing TBBM braking control and load-following hydraulic control, respectively (Figure 13). When combined, the fuel savings for the TBBM with load-following hydraulics were 24.1% and the CO_2e savings were 17.5%. These savings were achieved with minimal component modifications to the braking and hydraulic systems.

At a vehicle level, battery chemistries and charging strategies were explored to determine options that minimized CO_2e and cost. This study was performed because of the essential need to pursue options that reduce emissions due to current and future regulations [4] and because technologies with the lowest total cost of ownership (TCO) are more likely to be adopted [2]. This study found that LFP batteries provide the lowest TCO while also providing the lowest emissions, as seen in Figure 19, where the LFP chemistry with L2C in the U.S. emits 604 metric tons CO_2e at a TCO of $411,000, compared to the NCA chemistry with L2C in the U.S. at 831 metric tons CO_2e at a TCO of $1,019,000. This is mainly due to a much longer LFP battery lifetime, which can last several times longer than their NMC or NCA counterparts, as in Figure 14. The largest tradeoff comes from increased weight and space requirements from a lower energy density in the LFP battery.

The charging strategies compared L2C to opportunity DCFC. The best options for charging strategy are primarily dependent on the electricity grid emissions and the electricity demand charges. If using a cleaner electricity grid like in Oregon, the lifetime CO_2e emissions are much lower for the opportunity DCFC, with 329 metric tons CO_2e, compared to 544 metric tons CO_2e in the L2C case (Figure 19). Cost-wise, if there is a $0/kW demand charge, DCFC has a lower TCO at $383,000 in Oregon compared to the L2C at $404,000 (Figure 19). However, when including a demand charge of $30/kW (realistic in certain areas [37]), the DCFC has a much higher TCO at $953,000 compared to L2C at $418,000 (Figure 19).

The DCFC also enabled significant fuel consumption reductions along with notable CO_2e savings. In the case of the LFP battery using DCFC, the fuel savings were 71.5% and the CO_2e savings were 25.8% when compared to the plug-in series hybrid with an NMC battery and overnight L2C.

In this article, assumptions were made where data was unavailable or to facilitate quicker analysis. To further advance this work, the load-following hydraulics results could be verified on the plug-in series hybrid test platform. In its current form, the plug-in series hybrid is using an aggressive pedal map targeting peak regeneration and is also using load-following hydraulic control. The plug-in series hybrid is also being instrumented with a megawatt charging system connector to perform DCFC.

Acknowledgements

This material is based upon work supported by the U.S. Department of Energy's Office of Energy Efficiency and Renewable Energy (EERE) under the Vehicle Technologies Office (VTO) award number DE-EE0008800. The authors wish to thank John Terneus, Dr. Michael Weismiller, and Dr. Gurpreet Singh from the DOE for their continued support of this project. Also, thank you to the rest of the team at Pettibone for their everlasting assistance in providing technical information and invaluable insight with this project.

Contact Information

Bryant Goodenough, Ph.D., corresponding author
bgoodeno@mtu.edu

References

[1] F. Un-Noor *et al.*, "Off-Road Construction and Agricultural Equipment Electrification: Review, Challenges, and Opportunities," *Vehicles,* vol. 4, no. 3, pp. 780-807, 2022, doi: 10.3390/vehicles4030044.

[2] M. Thornton, M. Ratcliff, and K. Kelly, "Off-Road Vehicle Decarbonization and Energy Systems Integration: R&D Gaps and Opportunities," 2022, doi: 10.2172/1891267.

[3] R. Chen, C. Yang, Y. Ma, W. Wang, M. Wang, and X. Du, "Online learning predictive power coordinated control strategy for off-road hybrid electric vehicles considering the dynamic response of engine generator set," *Applied energy,* vol. 323, 2022, doi: 10.1016/j.apenergy.2022.119592.

[4] "Potential Amendments to the Off-Road New Diesel Engine Emission Standards: Tier 5 Criteria Pollutants and CO2 Standards." California Air Resources Board. https://ww2.arb.ca.gov/our-work/programs/tier5/about (accessed 09/05, 2024).

[5] W. Zhang, J. Wang, S. Du, H. Ma, W. Zhao, and H. Li, "Energy Management Strategies for Hybrid Construction Machinery: Evolution, Classification, Comparison and Future Trends," *Energies (Basel),* vol. 12, no. 10, p. 2024, 2019, doi: 10.3390/en12102024.

[6] B. Goodenough *et al.*, "Propulsion Electrification Architecture Selection Process and Cost of Carbon Abatement Analysis for Heavy-Duty Off-Road Material Handler," *SAE International Journal of Commercial Vehicles,* vol. 17, no. 3, 2024, doi: 10.4271/02-17-03-0014.

[7] W. Qiu *et al.*, "System configuration, control development, and in-field validation of a hybrid electric wheel loader featuring electrically-boosted engine," *Control Engineering Practice,* vol. 150, p. 105989, 2024/09/01/ 2024, doi: https://doi.org/10.1016/j.conengprac.2024.105989.

[8] X. Wang, Y. Huang, and J. Wang, "Study on Driver-Oriented Energy Management Strategy for Hybrid Heavy-Duty Off-Road Vehicles under Aggressive Transient Operating Condition," *Sustainability (Basel, Switzerland),* vol. 15, no. 9, p. 7539, 2023, doi: 10.3390/su15097539.

[9] H. Wang, Y. Huang, C. Lv, and A. Khajepour, "A Global Optimal Energy Management System for Hybrid Electric

off-road Vehicles," *SAE International journal of commercial vehicles,* vol. 10, no. 2, pp. 524-531, 2017, doi: 10.4271/2017-01-0425.

[10] W. Zhang, J. Wang, Z. Xu, Y. Shen, and G. Gao, "A generalized energy management framework for hybrid construction vehicles via model-based reinforcement learning," *Energy (Oxford),* vol. 260, 2022, doi: 10.1016/j.energy.2022.124849.

[11] H. Wang, Y. Huang, A. Khajepour, and Q. Song, "Model predictive control-based energy management strategy for a series hybrid electric tracked vehicle," *Applied energy,* vol. 182, pp. 105-114, 2016, doi: 10.1016/j.apenergy.2016.08.085.

[12] W. Zhang, J. Wang, Y. Liu, G. Gao, S. Liang, and H. Ma, "Reinforcement learning-based intelligent energy management architecture for hybrid construction machinery," *Applied energy,* vol. 275, p. 115401, 2020, doi: 10.1016/j.apenergy.2020.115401.

[13] C. Xiang, X. Hou, and Y. Ma, "Reinforcement learning-based active filter for the power management of off-road hybrid electric vehicles," in *CSAA/IET International Conference on Aircraft Utility Systems (AUS 2020)*, 18-21 Sept. 2020, pp. 53-58, doi: 10.1049/icp.2021.0172.

[14] P. Ponomarev, R. Åman, H. Handroos, P. Immonen, J. Pyrhönen, and L. Laurila, "High power density integrated electro-hydraulic energy converter for heavy hybrid off-highway working vehicles," *IET electrical systems in transportation,* vol. 4, no. 4, pp. 114-121, 2014, doi: 10.1049/iet-est.2013.0009.

[15] P. Y. Li, J. Siefert, and D. Bigelow, "A Hybrid Hydraulic-Electric Architecture (HHEA) for High Power Off-Road Mobile Machines," presented at the ASME/BATH 2019 Symposium on Fluid Power and Motion Control, 2019. [Online]. Available: https://doi.org/10.1115/FPMC2019-1628.

[16] D. Fassbender, Zakharov, Viacheslav, Minav, Tatiana, "Utilization of electric prime movers in hydraulic heavy-duty-mobile-machine implement systems," *Automation in construction,* p. 26, 2021. [Online]. Available: https://www.researchgate.net/publication/355031494_Utilization_of_electric_prime_movers_in_hydraulic_heavy-duty-mobile-machine_implement_systems.

[17] A. C. Mahato and S. K. Ghoshal, "Energy-saving strategies on power hydraulic system: An overview," *Proceedings of the Institution of Mechanical Engineers, Part I: Journal of Systems and Control Engineering,* vol. 235, no. 2, pp. 147-169, 2021, doi: 10.1177/0959651820931627.

[18] Y.-X. Yu and K. K. Ahn, "Optimization of energy regeneration of hybrid hydraulic excavator boom system," *Energy conversion and management,* vol. 183, pp. 26-34, 2019, doi: 10.1016/j.enconman.2018.12.084.

[19] W. Li, B. Cao, Z. Zhu, and G. Chen, "A novel energy recovery system for parallel hybrid hydraulic excavator," *TheScientificWorld,* vol. 14, 2014, doi: 10.1155/2014/184909.

[20] Y. Jong Il, K. Ahn Kyoung, and T. Dinh Quang, "A study on an energy saving electro-hydraulic excavator," 2009: IEEE, pp. 3825-3830.

[21] S. Qu, D. Fassbender, A. Vacca, and E. Busquets, "A High-Efficient Solution for Electro-Hydraulic Actuators with Energy Regeneration Capability " p. 25, 2020. [Online]. Available: https://www.researchgate.net/publication/345829033_A_High-Efficient_Solution_for_Electro-Hydraulic_Actuators_with_Energy_Regeneration_Capability.

[22] S. Qu, D. Fassbender, A. Vacca, and E. Busquets, "Formulation, Design and Experimental Verification of an Open Circuit Electro-Hydraulic Actuator," *IEEE,* 2020.

[23] D. Lovrec, M. Kastrevc, and S. Ulaga, "Electro-hydraulic load sensing with a speed-controlled hydraulic supply system on forming-machines," *International journal of advanced manufacturing technology,* vol. 41, no. 11-12, pp. 1066-1075, 2009, doi: 10.1007/s00170-008-1553-y.

[24] L. Huang, T. Yu, Z. Jiao, and Y. Li, "Research on Power Matching and Energy Optimal Control of Active Load-Sensitive Electro-Hydrostatic Actuator," *IEEE access,* vol. 9, pp. 51121-51133, 2021, doi: 10.1109/ACCESS.2020.3011629.

[25] Z. Yan, L. Ge, and L. Quan, "Energy-Efficient Electro-Hydraulic Power Source Driven by Variable-Speed Motor," *Energies (Basel),* vol. 15, no. 13, p. 4804, 2022, doi: 10.3390/en15134804.

[26] L. Ge, L. Quan, X. Zhang, B. Zhao, and J. Yang, "Efficiency improvement and evaluation of electric hydraulic excavator with speed and displacement variable pump," *Energy conversion and management,* vol. 150, pp. 62-71, 2017, doi: 10.1016/j.enconman.2017.08.010.

[27] A. Ghobadpour, H. Mousazadeh, S. Kelouwani, N. Zioui, M. Kandidayeni, and L. Boulon, "An intelligent energy management strategy for an off-road plug-in hybrid electric tractor based on farm operation recognition," *IET electrical systems in transportation,* vol. 11, no. 4, pp. 333-347, 2021, doi: 10.1049/els2.12029.

[28] C. Wei, X. Sun, Y. Chen, L. Zang, and S. Bai, "Comparison of architecture and adaptive energy management strategy for plug-in hybrid electric logistics vehicle," *Energy (Oxford),* vol. 230, p. 120858, 2021, doi: 10.1016/j.energy.2021.120858.

[29] B. Goodenough, A. Czarnecki, D. Robinette, J. Worm, P. Latendresse, and J. Westman, "Reducing Fuel Consumption on a Heavy-Duty Nonroad Vehicle: Conventional Powertrain Modifications," *SAE International Journal of Advances and Current Practices in Mobility,* vol. 6, no. 1, pp. 145-159, 2023, doi: 10.4271/2023-01-0466.

[30] P. Saiteja, B. Ashok, A. S. Wagh, and M. E. Farrag, "Critical review on optimal regenerative braking control system architecture, calibration parameters and development challenges for EVs," *International journal of energy research,* vol. 46, no. 14, pp. 20146-20179, 2022, doi: 10.1002/er.8306.

[31] X. Li and A. Jenn, "Energy, Emissions, and Cost Impacts of Charging Price Strategies for Electric Vehicles," *Environmental science & technology,* vol. 56, no. 9, pp. 5724-5733, 2022, doi: 10.1021/acs.est.1c06231.

[32] B. Borlaug, S. Salisbury, M. Gerdes, and M. Muratori, "Levelized Cost of Charging Electric Vehicles in the United States," *Joule,* vol. 4, no. 7, pp. 1470-1485, 2020, doi: 10.1016/j.joule.2020.05.013.

[33] L. Lanz, B. Noll, T. S. Schmidt, and B. Steffen, "Comparing the levelized cost of electric vehicle charging options in Europe," *Nature communications,* vol. 13, no. 1, pp. 5277-5277, 2022, doi: 10.1038/s41467-022-32835-7.

[34] Y. Preger *et al.*, "Degradation of Commercial Lithium-Ion Cells as a Function of Chemistry and Cycling Conditions," *Journal of the Electrochemical Society,* vol. 167, no. 12, 2020, doi: 10.1149/1945-7111/abae37.

[35] "eGRID 2021 Data." https://www.epa.gov/egrid/download-data (accessed 05/17, 2023).

[36] "Global EV Outlook 2024," International Energy Agency, 2024. Accessed: 08/09/2024. [Online]. Available: https://www.iea.org/reports/global-ev-outlook-2024/trends-in-electric-vehicle-batteries

[37] J. A. McLaren, P. J. Gagnon, and S. Mullendore, "Identifying Potential Markets for Behind-the-Meter Battery Energy Storage: A Survey of U.S. Demand Charges," United States, 2017. Accessed: 07/13/2023.

[Online]. Available: https://www.nrel.gov/docs/fy17osti/68963.pdf
[38] C. Rout, H. Li, V. Dupont, and Z. Wadud, "A comparative total cost of ownership analysis of heavy duty on-road and off-road vehicles powered by hydrogen, electricity, and diesel," *Heliyon,* vol. 8, no. 12, pp. e12417-e12417, 2022, doi: 10.1016/j.heliyon.2022.e12417.
[39] "GREET® Model: The Greenhouse gases, Regulated Emissions, and Energy use in Technologies Model," ed: Argonne National Laboratory, 2023.
[40] J. C. Kelly *et al.*, "Cradle-to-Grave Lifecycle Analysis of U.S. Light-Duty Vehicle-Fuel Pathways: A Greenhouse Gas Emissions and Economic Assessment of Current (2020) and Future (2030-2035) Technologies," 2022, doi: 10.2172/1254857.
[41] "The Emissions & Generation Resource Integrated Database," EPA, 2021. Accessed: 5/17/2023. [Online]. Available: https://www.epa.gov/egrid/egrid-technical-guide
[42] "eGRID 2022 Data." https://www.epa.gov/egrid/download-data (accessed 08/14, 2024).
[43] "Weekly Retail Gasoline and Diesel Prices." U.S. Energy Information Administration. https://www.eia.gov/dnav/pet/PET_PRI_GND_A_EPD2DXL0_PTE_DPGAL_A.htm (accessed 08/15, 2024).
[44] "Electric Sales, Revenue, and Average Price." U.S. Energy Information Administration. https://www.eia.gov/electricity/sales_revenue_price/ (accessed 08/15, 2024).

Definitions, Acronyms, Abbreviations

APP	Accelerator Pedal Position
BPP	Brake Pedal Position
CD	Charge Depleting
CO_2e	Carbon Dioxide Equivalent
DCFC	Direct Current Fast Charging
ICE	Internal Combustion Engine
KE	Kinetic Energy
L2C	Level 2 Charging, maximum of 19.2 kWh
LF	Load-Following
LFP	Lithium Iron Phosphate
LS	Load-Sensing
NCA	Nickel Cobalt Aluminum
NMC	Nickel Manganese Cobalt
OEM	Original Equipment Manufacturer
PTO	Power Take-Off
RB	Rule-Based
SOC	State of Charge
TBBM	Threshold-Based Brake Management
TCO	Total Cost of Ownership

Appendix A: Battery Parameters and Assumptions

Table A1. Full table of battery parameters and assumptions.

Parameter	NMC	NCA	LFP	Justification
Battery Lifetime Overnight L2 Charging	505 days	211 days	2215 days	Based on values from [34], assuming 20-80% SOC range at 25°C battery temperature and C-rate of 0.5. Adjusted to days of lifetime given SOC usage per day per chemistry. 18650 cells for all chemistries.
Battery Lifetime Opportunity DC Fast Charging	232 days	209 days	1177 days	Based on values from [34], assuming 0-100% SOC range at 35°C battery temperature and C-rate of 2. Adjusted to days of lifetime given SOC usage per day per chemistry. 18650 cells for all chemistries.
Battery Cost	$283/kWh	$232/kWh	$207/kWh	Assuming $250/kWh in 2021 from [6], where a low volume of batteries was expected due to a heavy-duty application. Then, this $250/kWh was adjusted for 2022 values based on IEA report [36].
Single Cell Peak Voltage	4.2 V	4.2 V	3.6 V	NMC value from manufacturer, NCA and LFP from Amesim.
Single Cell Capacity	4.74 Ah	2.95 Ah	2.4 Ah	NMC value based on calculation from known pack capacity and known number of cells in parallel. NCA and LFP from Amesim.
Pack Nominal Voltage	647 V	647 V	647 V	NMC value from manufacturer, NCA and LFP matching nominal voltage of NMC battery.
Pack Capacity	113.825 Ah	115.05 Ah	112.8 Ah	NMC value from manufacturer, NCA and LFP attempting to match capacity based on number of cells in parallel.
Pack Nominal Capacity kWh	73.6 kWh	74.4 kWh	73.0 kWh	Calculated based on pack capacity in Ah and nominal voltage.
Cells in Series	176	176	205	NMC from manufacturer, NCA and LFP based on matching peak voltage of NMC battery at 739.2 V.
Cells in Parallel	24	39	47	NMC from manufacturer, NCA and LFP based on matching pack capacity of NMC battery at 113.825 Ah.
Total Cell Mass	285 kg	312 kg	674 kg	Taking cell mass times number of cells. Cell mass for NMC from manufacturer, and NCA and LFP from Amesim. LFP much lower energy density, hence higher mass.
Total Cell Volume	0.13 m^3	0.12 m^3	0.33 m^3	Cell volume calculations based on density values in Amesim for each battery chemistry. This includes cell volume only.
Total Pack Assembly and Bill of Materials CO_2e	150 kg CO_2e/kWh	159 kg CO_2e/kWh	294 kg CO_2e/kWh	Using GREET 2023 [39] for GHG-100 values for each architecture, including total lithium ion assembly process emissions and lithium ion bill of materials emissions. NMC811 values used.

Appendix B: CO_2e and Cost Assumptions

Table B1. Full table of CO_2e and cost assumptions. See [6] for assumptions for similar analysis.

Category	Assumption	Justification
Lifetime of Cary-Lift	15 years	15-year lifetime in [40].
Electricity Grid CO_2e	Average mix	Average mix recommended by EPA [41]. Values for emissions come from eGRID using the most recently available 2022 values [42].
Demand Charges on Electricity	$15/kW unless otherwise stated	Estimated from NREL report [37], but values vary widely per region and provider.
Charging Efficiency	90%	Assumption for average charging efficiency for grid charging.
Maintenance CO_2e	Only considered for battery replacements	Maintenance for events like engine rebuilds and axle rebuilds unknown. Replacement of electric machines does not happen in 15-year lifetime. Battery replacements are also higher source of emissions than other components, driving up CO_2e and making battery replacements important to include.
Maintenance Cost	Cost based on market prices for products, informed by discussions with Pettibone	Maintenance and replacements costs can vary, hence assistance of Pettibone in cost of replacement and rebuilding of components.
Cost Increase to Customer	Twice as expensive to customer as to manufacturer	Based on discussions with Pettibone, parts can be twice as expensive to customers than to manufacturers. This will vary with manufacturer. Battery replacement costs are assumed twice as expensive to customer than to Pettibone.
CO_2e Values over Lifetime	Does not change	Assuming a constant CO_2e emissions over the lifetime of the machine for simplicity and due to unknown future values.
Cost Values over Lifetime	Does not change	Assuming constant cost in 2022 dollars, for simplicity and due to unknown future values.
CO_2e of Diesel by Geographic Region	Does not change	Values are available from GREET [39] for U.S., but do not specify per state.
Cost of Diesel by Geographic Region	Changes by state	Cost available by state from EIA [43].
CO_2e of Electricity by Geographic Region	Changes by state	CO_2e available by state from eGRID [42].
Cost of Electricity by Geographic Region	Changes by state	Electricity cost available by state from EIA [44].
Control of Plug-in Series Hybrid	Baseline regenerative braking strategy with continuously spinning hydraulics	Assuming the most simple form of control. This enables readers to understand fuel, cost, and CO_2e savings in an application without the use of more complicated control schemes.
Operator break time for opportunity DC fast charging	Two 10-minute breaks and one 30-minute lunch break	Assuming operator takes a 30-minute lunch break and two 10-minute breaks during an 8-hour shift. Actual break times will vary.
Cost of charging infrastructure	Charging infrastructure cost not considered	Charging infrastructure costs vary and are outside of the scope of this work. Installing a DC fast charger is likely to be much more expensive than a Level 2 charger.
Charging strategy operating cycle	Time-weighted operating cycle shifted to include idle periods during breaks	Original time-weighted operating cycle has entire idle period at end of cycle. This was modified so these idle periods occur earlier in the cycle during breaks. Idle time reduced at the end of cycle because of the use of idle time for breaks.